TM-1013
7184.605
2125.000
November 1980

LONGITUDINAL SHOWER DEVELOPMENT IN A LEAD-SCINTILLATOR CALORIMETER AS A TOOL TO SEPARATE PIONS AND ELECTRONS AT 10-50 GEV ENERGIES*

Y. Sakai, B.C. Brown, D. Finley, J. Hanson, Y. Hemmi, A. Ito, H. Jostlein, A. Maki, and K. Sugano

Kyoto University, Fermi National Accelerator Laboratory, National Laboratory for High Energy Physics--KEK, State University of New York at Stony Brook, University of Washington/Seattle

*Supported by Japan Society for Promotion of Science, U.S. Department of Energy, and National Science Foundation.

Introduction

Since multi-hundred GeV particle accelerators have been built for high energy physics research, calorimetry has become a very important method not only for measuring particle energy but also for identifying particle species. Consequently, there has been a tremendous amount of effort expended in understanding the electromagnetic shower and hadronic cascade phenomena, and a good knowledge of these phenomena now exists.[1] However, the practical design of a calorimeter for a specific application usually reveals gaps in this knowledge, especially in regard to hadron rejection in an electromagnetic shower calorimeter.

A versatile shower counter based on a lead-scintillator sandwich design was constructed and tested in order to determine the optimal design for hadron rejection in an electromagnetic shower detector which will be used in Fermilab Experiment 605.

Experimental Arrangement

The small lead scintillator shower counter was built and tested at Fermilab. The detector is shown in Fig. 1 and consisted of 40 layers of lead and plastic scintillator. The lead plates were all 8" x 8" and 1/8" thick. The scintillators were 1/4" thick NE102 (8" x 8") and NE110 (6" x 8"), and grouped into 10 segments: from upstream to downstream, 4, 4, 2, 2, 2, 2, 2, 2, 10 and 10 layers (Table 1). Each segment was viewed through a Lucite light guide by a phototube. The first two segments were viewed by RCA6655A phototubes, the last two by RCA8055 phototubes, and the remaining six by RCA6342A phototubes. The entire detector was placed in a light tight wooden box.

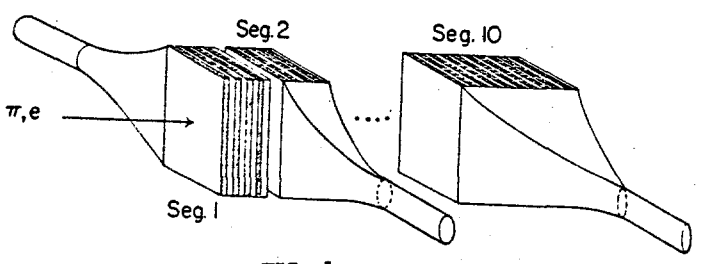

FIG. 1

The 15-45 GeV/c π^- and e^- in the unseparated M5 beam were used to investigate the electron resolution and hadron rejection of the shower counter. The momentum spread of the beam was measured by a lead glass counter to be less than 1%. The electron trigger required a coincidence signal from three scintillation trigger counters (U,D,T), two threshold gas Cherenkov counters (C_1, C_2), and a hole counter (V) in veto: $(U.D.C_1.C_2).(T.\bar{V})$. The pion trigger used the gas Cherenkov counters as a veto instead of coincidence: $(U.D.\bar{C}_1.\bar{C}_2).(T.\bar{V})$. The T counter (1 cm wide, 2 cm high) was the smallest defining counter and was located 5 m upstream of the calorimeter.

The species composition of the beam was idependently measured by changing the pressure of C_1. It was found that e:μ:π: other heavier particles = 2.4%: 2.2%: 86.8%: 8.6% at 30 GeV. These measurements demonstrate that muons in the pion trigger have a negligible effect on the results when compared to the accuracy of the hadron rejection measurements.

The efficiency of the Cherenkov counters for electrons was measured at various pressures of the gas. Due to the low efficiency of the gas Cherenkov counters, especially at higher energies, electrons remaining in the pion trigger can apparently reduce the measured value of the hadron rejection factor. In order to investigate this, a wedge-shaped lead brick was installed at the first focusing point of the beam line, immediately in front of the momentum slit. This lead brick reduced the electron fraction in the beam to the order of 10^{-5} without using Cherenkov counters in veto, but it also reduced the intensity of the hadron beam by about a factor of 10. A nearly pure hadron beam was achieved by requiring, in addition, the Cherenkov counters in veto; in this case, the fraction of electrons remaining in hadron trigger ranged from 1×10^{-6} at 20 GeV to 1×10^{-5} at 45 GeV.

Hadron rejection measurements were done for three beam energies (30, 40 and 45 GeV) and for three different thicknesses of lead plate placed immediately in front of the shower counter. Electron spectra were taken before and after each hadron run with the same detector configuration. These electron measurements together with hadron data sliced into many time periods monitored the long term gain variation of the phototubes.

Electron Energy Resolution

Data were taken at electron energies from 15 GeV to 45 GeV with various thicknesses of lead plate in front of the shower counter. The phototube gain of each segment was calibrated by using electron data with no lead plate in front of the shower counter. The total energy deposit in the shower counter is given for each event by

$$E_{tot}(i) = \sum_{j=1}^{N_{pm}} E_j(i) = \sum_{j=1}^{N_{pm}} a_j \, (X_j(i) - P_j)$$

where $E_j(i)$ is the energy deposit in the j-th segment; $X_j(i)$ is the ADC channel number, P_j is the pedestal channel, and a_j (GeV/channel) is the relative gain to be determined for each phototube. a_j was determined by minimizing the rms width of the total energy distribution E_{tot}. The distribution of the total

energy deposit for electrons with various conditions was fitted by a Gaussian distribution over the range of 3 standard deviations around the peak. These relative phototube gains were in reasonably good agreement within experimental error for different energies without the front lead plate, and will be called "nominal" gains.

Using the nominal gains the means (μ) and energy resolutions (σ/μ) were evaluated for various electron energies and lead plate thicknesses. These are shown in Fig. 2 for the case of no front lead plate. The linearity of the mean against the electron energy is fairly good. The dashed curve drawn in the figure is

$$\frac{\sigma}{\mu} = 11.5\% / \sqrt{E} \quad (E = \text{energy of electron in GeV}).$$

This curve represents the data well.

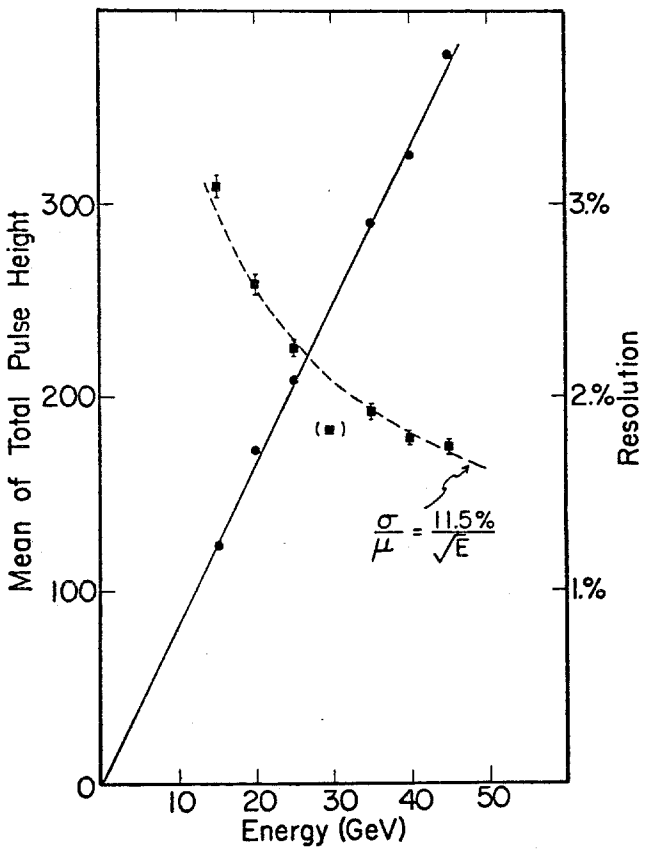

FIG. 2

The resolution at 30 GeV is appreciably below the dashed curve. However, these data were taken with higher voltages supplied to the phototubes than those for all other energies. The apparent discrepancy could come from the different effective quantum efficiencies of the photocathode at different high voltages. This effect is especially apparent when voltages are supplied to phototubes excessively lower than their nominal working voltages.

The means and energy resolutions are shown in Fig. 3 for the case of lead plates in front of the shower counter. As more lead is placed in front of the shower counter, the total pulse height becomes lower and the electron energy resolution becomes worse. For the same lead thickness the decrease in pulse height for higher energies is a smaller effect, as expected. However, no clear energy dependence of the deterioration of energy resolution due to the addition of the front lead was found.

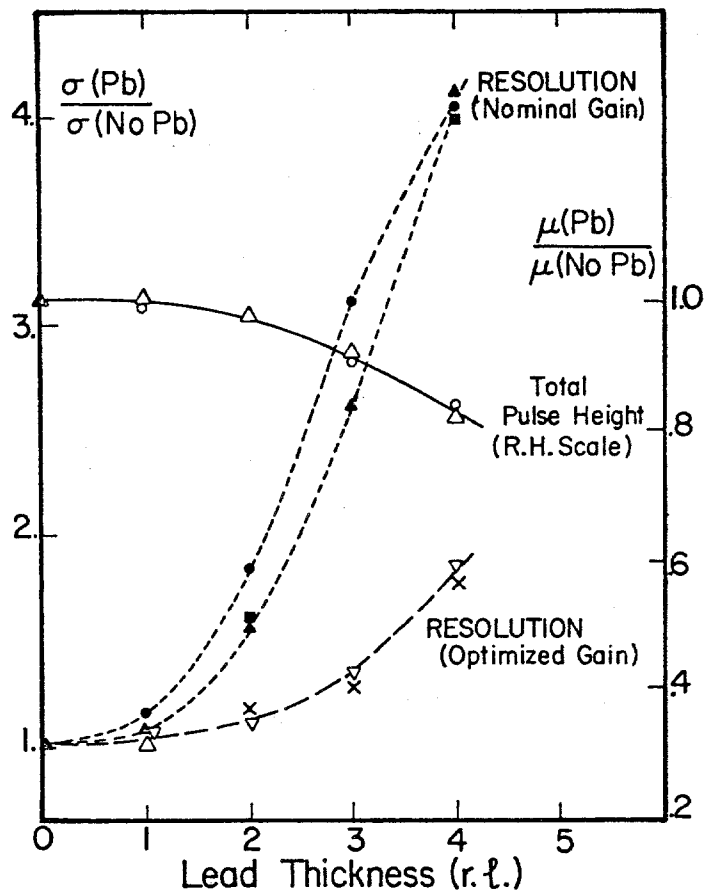

FIG. 3

The missing information (energy loss in the front lead plate) can be restored to some extent by changing the gains artificially, and the energy resolution can be consequently improved by more than a factor of 2. Table 2 shows examples of relative phototube gains which minimize the energy resolution for the case of 2 or 4 r.l. in the front lead plate at 45 GeV and compares them to the nominal gains. The minimization assigns a larger weight in the first segment with the thicker front lead plate. It is concluded that the energy deposit in the first segment is strongly correlated to the energy loss in the front lead plate, and the assignment of a larger weight to the first segment compensates largely for the invisible energy lost in the front lead plate.

Hadron Rejection

Hadron rejection by the shower counter was investigated by comparing the hadron energy distribution deposited in each segment to the corresponding distribution for electrons. The electron inefficiencies and the hadron rejection factors were estimated for various levels of cuts assumed in the pulse height distributions.

In some cases, events overflowed the ADC in the 9th and 10th segments. Therefore, in the analysis of the data, it was required, in advance of any other cuts, that pulse heights from the 9th and 10th segments were both less than the 1100 channel of the ADCs. These cuts eliminated about 10% of pion events, 4.6% and 1% of 45 GeV electrons with zero and 2 r.l. of front lead, respectively, and negligible amounts of other electron events. The ADC overflow cut does not significantly affect the final hadron rejection factor, but it does, of course, increase the electron inefficiency by the small amounts mentioned above.

These effects are not taken into account in the present analysis; nevertheless, the conclusions remain the same. The rejection factor using a total energy cut only was about half that of the combined cut of segments 9 and 10 and total pulse height.

1) Cut by Total Pulse Height

Fig. 4 shows the plots of electron inefficiency versus the hadron rejection factor for various widths of cut in the total pulse height distribution (E_{tot}). The cuts are symmetric around the mean value of the electron pulse height distribution. The lead in front of the shower counter makes the electron resolution worse, and consequently decreases the hadron rejection factor.

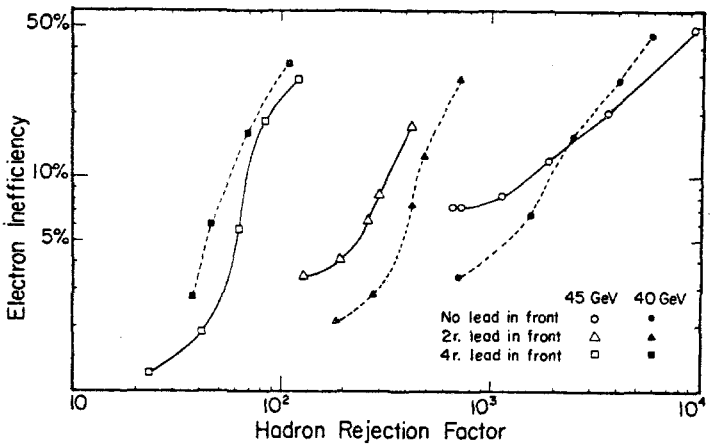

FIG. 4

2) Cut by Each Segment in Addition to Total Pulse Height Cut.

After the cut by total pulse height, the pulse height distributions in each segment for 45 GeV electrons and pions are shown in Fig. 5 for various thicknesses of the front lead (a) no lead; b) 2 r.l.; c) 4 r.l.). It is clearly seen that better hadron rejection can be achieved by requiring an additional cut in individual segments. This is especially apparent in the case of b) and c) in Fig. 5.

Various segments or combinations of segments were used in addition to the total pulse height cut of $\pm 2\sigma$ and $\pm 4\sigma$. The results are shown in Fig. 6 and Fig. 7. The following are observed in the figures.

(i) The first segment gives the most efficient rejection among any single segment or any combinations of segments.

(ii) Comparing the curves of segment 1, segment 1+2 and segment 1+2+3, it is observed that thinner first segments give better rejection, although there should obviously be an optimum thickness between zero and 2 r.l.

(iii) Fig. 7b shows that at a fixed electron inefficiency, one can get better hadron rejection by first requiring a strict cut in total pulse height and then in the first segment, rather than first requiring a loose cut in total pulse height and then a strict cut in the first segment.

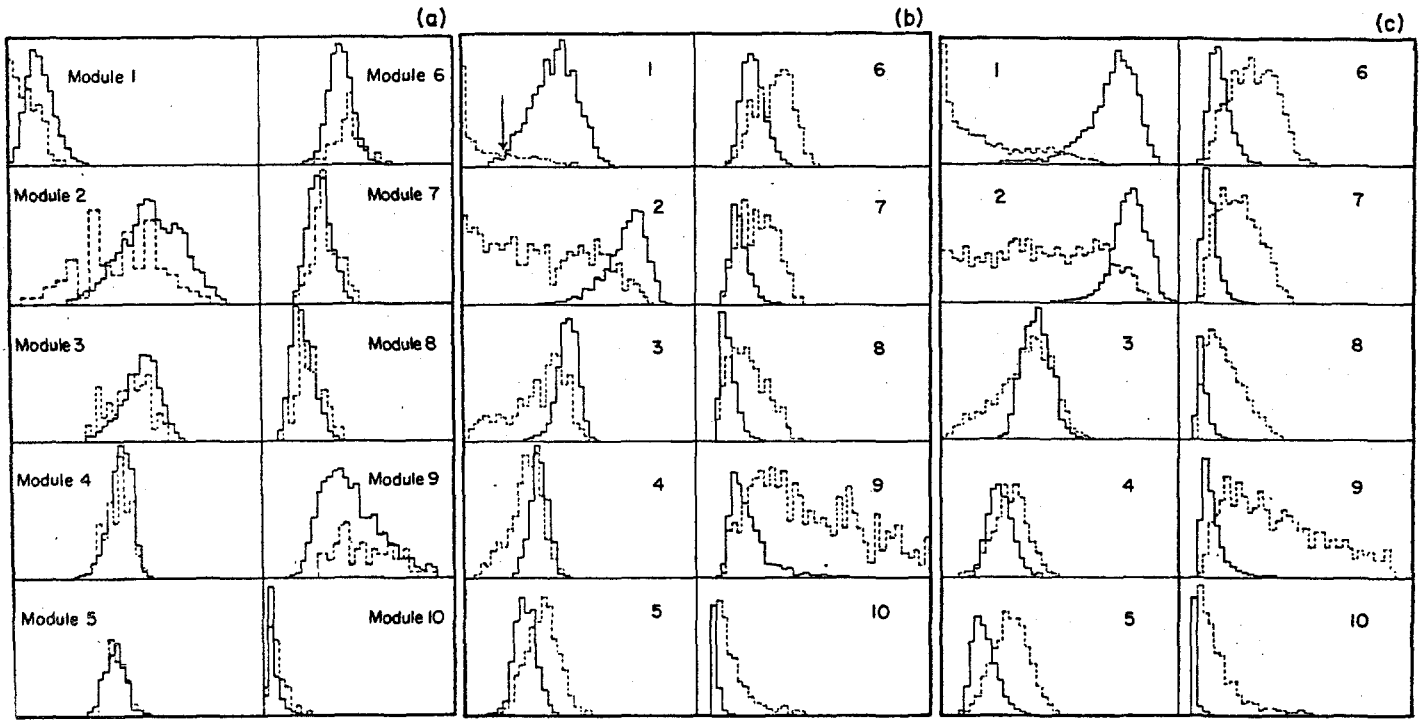

FIG. 5

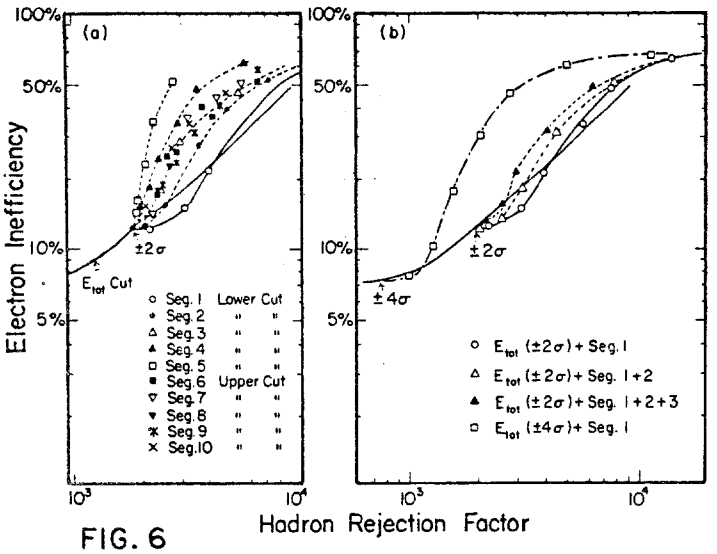

FIG. 6

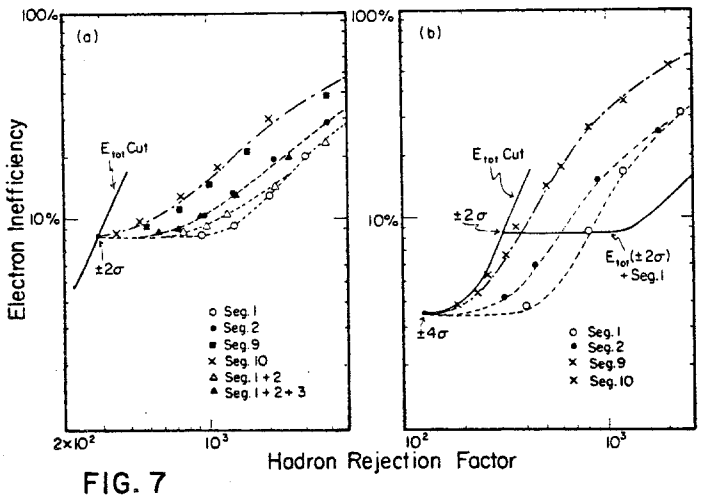

FIG. 7

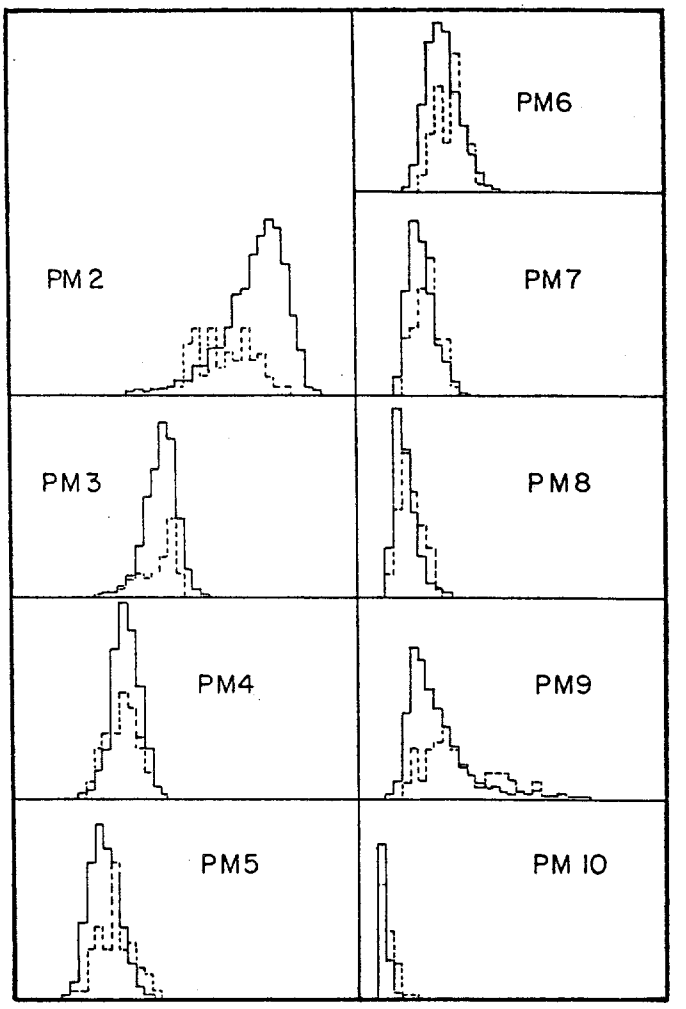

FIG. 8

Additional cuts using other segments do not give further hadron rejection since the pulse height in the first segment is strongly correlated to the pulse height of other segments for the pion events which have passed the E_{tot} cut. The E_1 cut eliminates most events outside the electron region in other segments. This is clearly seen in Fig. 8 which shows the pulse height distribution in each segment of the events passing the E_{tot} cut ($\pm 2\sigma$) and the E_1 cut shown by the arrow in Fig. 5(b). The additional cut using other segments gives no additional hadron rejection. This is shown quantitatively in Fig. 9.

Fig. 10(a) shows the electron inefficiency versus the hadron rejection factor using the total pulse height cut and the segment 1 cut for various lead thicknesses at 45 GeV.

It is also seen from the pulse height distribution in Fig. 5(a)~(c) that as the second cut after the E_{tot} cut, the E_1 cut is more efficient in the hadron rejection for the thicker front lead than for thinner or no front lead. However, at fixed energy, the final rejection factor obtained by these two cuts is smaller for thicker lead at a 10% electron inefficiency level. This is different from the lead glass case due to the different dependence of electron resolution on the lead thickness. In our case the front lead plate deteriorates the resolution even if it is 2 r.l., and consequently decreases the rejection factor. In case of the lead glass, on the other hand, no difference is observed in resolution between no lead and 2 r.l. of lead, and therefore the hadron

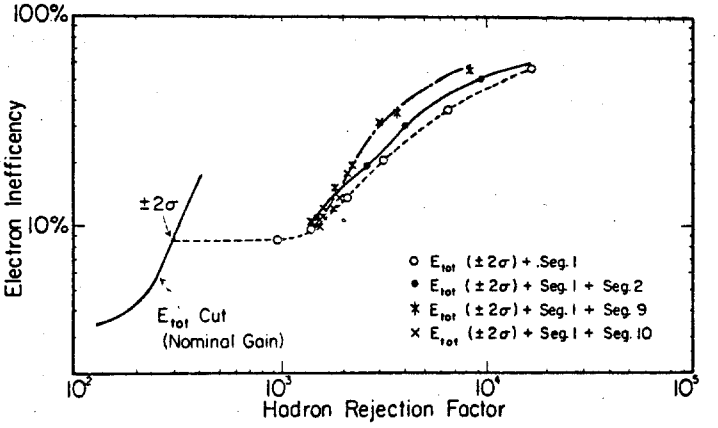

FIG. 9

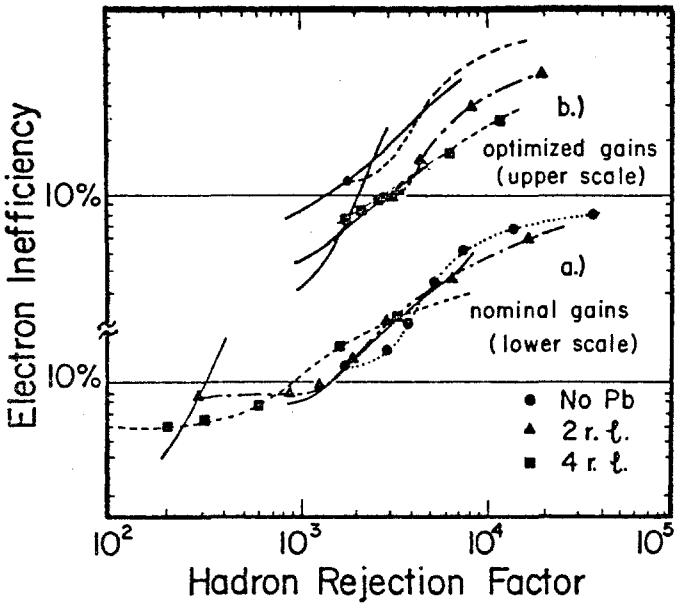

FIG. 10

rejection using the E_{tot} cut remains almost constant regardless of the lead thickness.[2]

(3) Optimized Gains

As described above, better resolutions for the configurations with some front lead can be achieved by adjusting the gains artificially. The results using these "optimized" gains are shown in Fig. 11. Here, the hadron rejection using the E_{tot} cut is greatly improved , and additional cuts by individual segments is not as effective as in the case of the nominal gains. As in the case of the nominal gains, the most efficient cut in addition to the E_{tot} cut is the E_1 cut, although it is not as dramatic. No additional hadron rejection can be gained using any other segment nor any combination of the other segments.

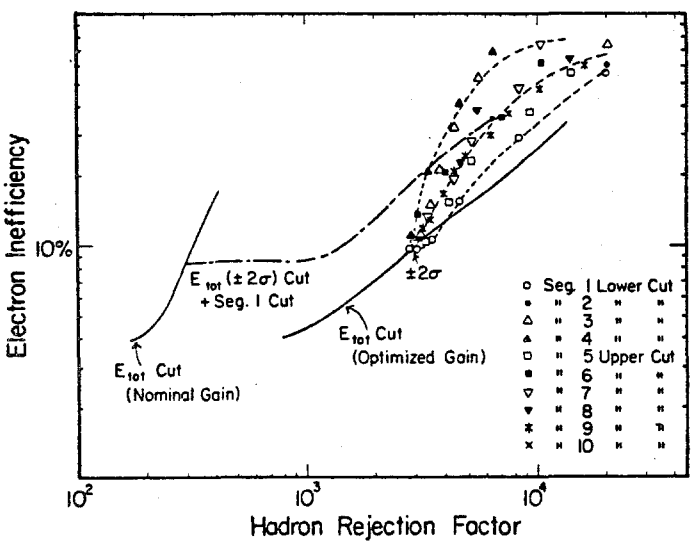

FIG. 11

Since the optimized gains assign more weight to the first segment, the E_{tot} cut not only uses the total energy deposit in the shower counter but also the information about energy deposit in the first segment. Consequently, the additional cut using the first segment is not as effective as in the case of the nominal gains. However, at the highest energy, the front lead plates improve the hadron rejection and give a better rejection factor than the case with nominal gains and with no lead plate in front (Fig. 10(b)).

Conclusion

We have investigated electromagnetic showers and hadron cascades in a lead plastic scintillator sandwich counter. We have found that this counter can give very good hadron rejection by using the information on the total energy deposit and the energy deposit in the first thin segment. Additional lead in front of the counter combined with the optimized phototube gains improves the hadron rejection. With this configuration and method of analysis, a factor of 3500 rejection was obtained for 45 GeV π^- at a cost of a 10% electron loss. Further segmentation of the counter in the downstream section provides little improvement in hadron rejection.

Acknowledgement

We wish to thank Rich Krull for the fabrication of the optical systems, and other members of the E605 collaboration for their help and encouragement during the test.

References

1) Seigi Iwata, Nagoya University DPNU-13-80, May 1980, and references in this article (Unpublished).
2) J.A. Appel et al., Nuclear Instruments and Methods 127 (1975) 495.

Figure Captions

Fig. 1. Detector configuration. Forty layers of lead and scintillator sheets were grouped into 10 segments, each of which was viewed through an acrylic light guide by a phototube. Segmentations were 4 layers (Seg 1 and 2), 2 layers (Seg 3 to 8) and 10 layers (Seg. 9 and 10). The entire detector was placed in a light tight wooden box.

Fig. 2: Energy dependence of the total pulse height and energy resolution. The energy resolutions are well represented by a scaling formula $\sigma/\mu = 11.5\%/\sqrt{E}$ (E: energy in GeV).

Fig. 3: Dependence of the pulse height and energy resolution on the thickness of the lead plate placed in front of the shower counter for beam energies of 45 (circle), 40 (triangle) and 30 GeV (rectangle). x and ∇ are the energy resolution with optimized gain (see text) for 45 and 40 GeV respectively.

Fig. 4: Electron inefficiency versus hadron rejection factor using the cut in the total pulse height distribution obtained with the nominal gains (see text).

Fig. 5: Energy distribution deposited in each segment by 45 GeV electrons (solid line) and hadrons (dashed line) which passed the total energy cut of ±2 standard deviations around electron peak for the case of (a) no front lead, (b) 2 r.l. front lead, and (c) 4 r.l. front lead.

Fig. 6: Additional cuts for no front lead after total energy cut of ±2 standard deviations with various segments (a) and combinations of segments (b). Total energy cut of ±4 standard deviations plus segment 1 is shown in (b).

Fig. 7: Similar to Fig. 6 but for 2 r.l. front lead. Total energy cuts are at ±2 standard deviations (a) and at ±4 standard deviations (b).

Fig. 8: Energy distribution with two r.l. of front lead in segments 2 to 10 deposited by 45 GeV electron (solid line) and pion (dashed line) events passing the total energy (±2σ) and E_1 cut.

Fig. 9: Third cuts after total energy and E_1 cuts. Note that no single cut can exceed the stricter E_1 cut.

Fig. 10: Electron inefficiency versus rejection factor at 45 GeV obtained by the total energy cut plus E_1 cut for various amounts of front lead in the case of the nominal gains (a), and of the optimized gains (b).

Fig. 11: Comparison of the rejection factors with the optimized gains to those with the nominal gains for 45 GeV and 2 r.l. front lead.

TABLE I

Detector configuration

Segment*	#of layer	Thickness in r.l.	Thickness in a.l.	Integrated Thickness in r.l.	Integrated Thickness in a.l.
1	4	2.33	0.106	2.33	0.106
2	4	2.33	0.106	4.66	0.212
3	2	1.16	0.053	5.82	0.265
4	2	1.16	0.053	6.98	0.318
5	2	1.16	0.053	8.14	0.371
6	2	1.16	0.053	9.30	0.424
7	2	1.16	0.053	10.46	0.477
8	2	1.16	0.053	11.62	0.530
9	10	5.82	0.265	17.44	0.795
10	10	5.82	0.265	23.26	1.060

Table 2 - Examples of Phototube Gain

$$E_{tot} = \sum_{j=1}^{N_{pm}} a_j E_j$$

a_j	45 GeV (2 r.l. Pb) Nominal	45 GeV (2 r.l. Pb) Optimized	45 GeV (4 r.l. Pb) Nominal	45 GeV (4 r.l. Pb) Optimized
a_1	1.472	2.315	1.594	5.244
a_2	1.349	1.308	1.390	.9643
a_3	1.118	1.152	1.126	1.271
a_4	.8690	.7296	.8346	1.012
a_5	1.	1.	.8865	1.
a_6	.7788	.5618	.7596	.8129
a_7	.6789	.6690	.6736	1.079
a_8	.5403	.6069	.5587	.9939
a_9	.7907	.8850	.9421	1.321
a_{10}	.5841	-0.1827	.6160	-0.4295
Resolution	3.200%	1.908%	7.066%	3.217%